J Biol Inorg Chem (2009) 14:1119–1128
DOI 10.1007/s00775-009-0556-y

ORIGINAL PAPER

Molecular dynamics simulations of mouse ferrochelatase variants: what distorts and orientates the porphyrin?

Borys Szefczyk · M. Natália D. S. Cordeiro · Ricardo Franco · José A. N. F. Gomes

Received: 17 March 2009 / Accepted: 9 June 2009 / Published online: 20 June 2009

Abstract Molecular dynamics simulations of the wild-type and variant forms of the mouse ferrochelatase in complex with the product (haem) have been performed using the GROMOS96 force field, in the NpT ensemble. Ferrochelatase, the last enzyme in the catalytic pathway of the haem biosynthesis, catalyses the reaction of insertion of a ferrous ion into protoporphyrin IX by distorting the planar geometry of the latter reactant. The simulations presented aim at understanding the role of active-site residues in this catalytic process. Analysis of the simulation trajectories explains the consequences of the mutations introduced and sheds more light on the role of the His209 residue in porphyrin macrocycle distortion. The function of residues coordinating propionate groups of the haem molecule is discussed in terms of stability of the substrate and product complexes.

Keywords Haem · Heme biosynthesis · Chelatase · Mutagenesis · Iron metabolism

Electronic supplementary material The online version of this article (doi:10.1007/s00775-009-0556-y) contains supplementary material, which is available to authorized users.

B. Szefczyk (✉) · M. N. D. S. Cordeiro · J. A. N. F. Gomes
REQUIMTE, Department of Chemistry,
Faculty of Science,
University of Porto,
Rua do Campo Alegre 687,
4169-007 Porto, Portugal
e-mail: borys.szefczyk@fc.up.pt

B. Szefczyk
Institute of Physical and Theoretical Chemistry,
Wrocław University of Technology,
Wybrzeże Wyspiańskiego 27,
50-370 Wrocław, Poland

R. Franco
REQUIMTE, Department of Chemistry,
Faculty of Science and Technology,
New University of Lisbon,
2829-516 Caparica, Portugal

Introduction

The haem molecule is widely considered to be vital, owing to its role as a cofactor in haemoglobin. However, its function is much wider; for instance, haem can be found as a cofactor in cytochromes (e.g. in cytochrome P450s [1], a family of enzymes responsible for metabolizing endo- and exogenous compounds, including, e.g., drugs), it plays a role in gene transcription [2] and it is also one of the factors involved in metabolic perturbations in Alzheimer's disease. [3] The last step of the biosynthesis of haem, namely insertion of the ferrous ion (Fe^{2+}) into the protoporphyrin IX (PPIX) molecule (Fig. 1), is catalysed by ferrochelatase [4]. Due to this key role, ferrochelatase can be found in bacteria and eukaryotes, including plants and animals [5, 6]. This versatility and crucial function for living organisms renders it an important object of study. The generally acknowledged mechanism of the reaction involves the following steps: binding of PPIX, distortion of the macrocycle, metal ion insertion, which results in an increased stiffness of the porphyrin, and product release [7, 8, 9]. This mechanism is supported by experimental and theoretical results: X-ray characterization of several wild-type (WT) and variant forms of ferrochelatase, free or in the complex with substrate, product and inhibitors [9, 10, 11, 12], mutagenetic studies [8, 13, 14] and molecular modelling [15]. Nevertheless, the role of the active-site residues in the subsequent phases of the reaction and, in particular, in

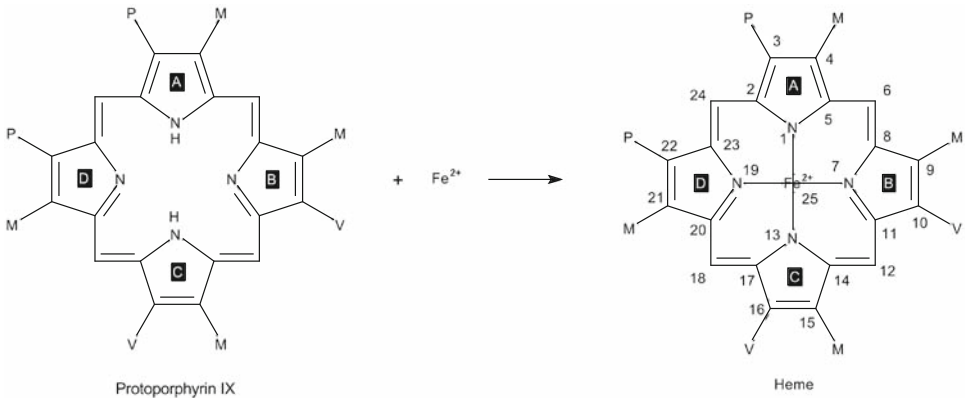

Fig. 1 Reaction catalysed by ferrochelatase. Pyrrole ring symbols (*A*, *B*, *C*, *D*) and the atom numbering used in this paper (*1–25*) are shown. *M* methyl, *V* vinyl, *P* propionyl

the macrocycle distortion is not quite clear. Franco et al. [13] have studied WT and variants of the mouse ferrochelatase—H209N and E289Q—by means of resonance Raman and UV–vis spectroscopy and concluded that these mutations affect the amount and type of the macrocycle distortion. E289A and E289Q variants of recombinant mouse ferrochelatase were found to contain endogenous and specifically bound PPIX. Differential scanning calorimetry [16] and product release kinetic studies [17] of those variants indicated that they exhibited enhanced protein stability when compared with WT ferrochelatase, and that Glu289 appears to be critical for the mouse ferrochelatase catalytic process, by controlling the release of the product. In *Bacillus subtilis* ferrochelatase, His183 and Glu264 (corresponding to His209 and Glu289 in mouse ferrochelatase) have been shown to represent the metal binding site of the enzyme [18]. Recently, Karlberg et al. [12] have shown that the *B. subtilis* ferrochelatase distorts the porphyrin in a way similar to the mouse enzyme [14] and that the primary function of His183, in addition to porphyrin distortion, is metal binding and its insertion into the macrocycle; the latter indirectly via proton abstraction. This is despite the fact that the sequences of bacterial and mammal ferrochelatase have only 24% similarity, with His209 being one of the few invariant residues in the ferrochelatase family [5]. Quantum mechanics/molecular mechanics calculations by Sigfridsson and Ryde [15] show that the distortion of the protoporphyrin after the metal insertion costs much more energy than the distortion of a free-base protoporphyrin. This result was observed for several ions, except Cd^{2+}, which is an inhibitor of ferrochelatase [19]. Such studies motivated us to look more closely at the role of the active-site residues in protoporphyrin distortion. On the basis of the X-ray structure of human ferrochelatase [9] it is clear that Met76 and His263 (His209 in mouse) are in a position to coordinate the iron atom. A similar model emerges from the present study, although a covalent linkage is not considered. Molecular modelling and the molecular dynamics (MD) method allow to study the structure of various forms and complexes of ferrochelatase at the atomic level and analyse the changes in the structure caused by mutations; therefore, they are well suited to study this problem. In this work, we choose to focus on three forms of the ferrochelatase isolated from mouse (*Mus musculus*; MFCh), namely WT, H209N and E289Q, complexed with the product of the reaction—the haem molecule. MD simulations are applied to study the influence of the mutations on the structure of the monomeric form of the protein and the planarity of the haem molecule. On the basis of these results, we draw conclusions concerning the role of the porphyrin macrocycle distortion and the function of several residues.

Methods

Homology modelling

The crystal structure of MFCh has not been resolved yet, therefore the coordinates of this protein were determined using the homology modelling technique, implemented in the MODELLER program [20]. The sequence of MFCh, deposited in the Swiss-Prot database (record Q3UC49) [21], was aligned with the sequence of chain A of the human ferrochelatase taken from Protein Data Bank (PDB) record 2HRC (P22830 in Swiss-Prot) [9]. Note that the initial 64 residues (63 in mouse) of the sequence [21] represent a mitochondrial targeting sequence, removed in the proteolytic processing and therefore not present in the X-ray structure (nor in the models shown here). The similarity of the human and mouse sequences is very high (92%), with no insertions or deletions, ensuring that the final structure of MFCh is reliable (Fig. 2). On the basis of the X-ray coordinates of human ferrochelatase (2HRC), five initial models of MFCh were generated in MODELLER and the model with the lowest molecular probability density function (PDF) value was selected for future use. The discrete optimized protein energy (DOPE) score of this model was evaluated and no indication of incorrect structure was found (Fig. S1). Additionally, the final

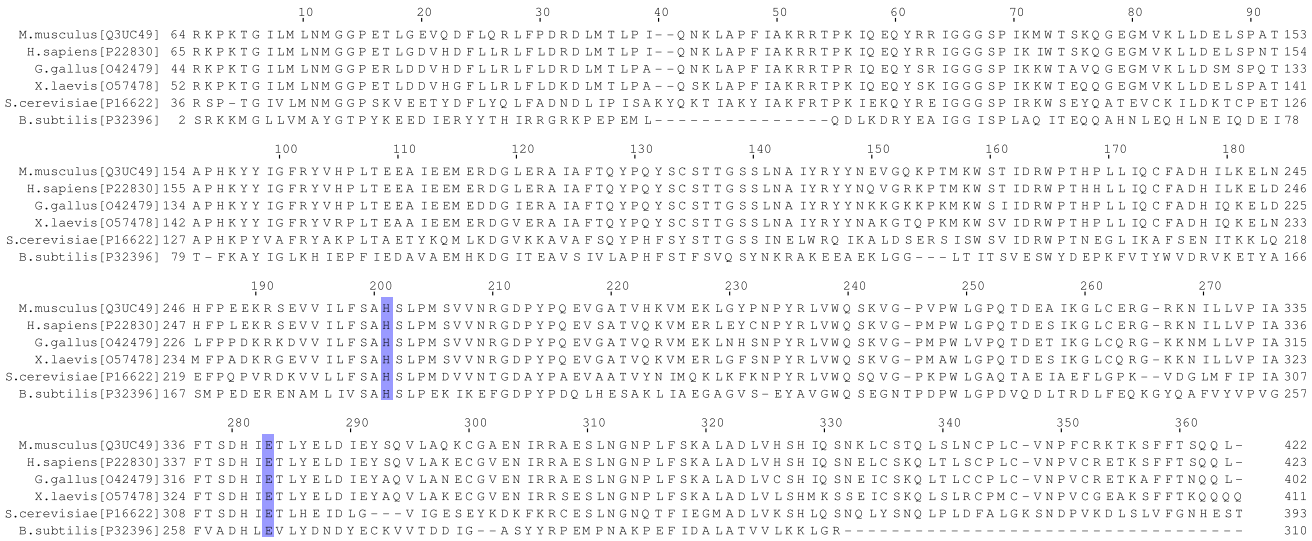

Fig. 2 Alignment of the ferrochelatase sequence from various organisms. Swiss-Prot record numbers are given in *brackets*. *Coloured boxes* indicate the catalytic residues, His209 and Glu289. Note that only the part of the sequence modelled in this study (359 amino acids) is shown. Sequence alignment was performed using the ClustalW [41] Web server and visualized in Jalview [42]

models of MFCh were verified using the PROCHECK program [22] and were found to be valid. Models of the variants, H209N and E289Q, were prepared in a similar manner, starting from the sequence taken from the Swiss-Prot database with substituted residues. Residues 209 and 289 correspond to residues 207 and 287, respectively, in [13] and to residues 263 and 343, respectively, in [8, 9].

Most eukaryotic ferrochelatases contain a [2Fe–2S] cluster. It has been experimentally proven that this cluster is present in the structure of MFCh and human ferrochelatase [5]. However, there is no evidence for the cluster being involved in the reaction and its position in the protein structure is far away from the active site. For that reason, the [2Fe–2S] cluster was not included in the models used here. Additionally, there is a possibility of forming a disulphide bridge between Cys269 and Cys306. Such a bridge can be observed in two (out of four) chains in the 2QD1 X-ray structure, in the PDB [9], but it is not present in other structures of ferrochelatases (see, for example, records 1HRK, 2HRC, 2QD2, 2QD3, 1QD4) [9, 11]. In the models presented here, the cysteines in question were terminated with thiol groups and therefore the disulphide bridge is not present.

To insert the haem molecule, each model was aligned with an X-ray structure containing PPIX (record 2QD1 in the PDB) [23], the protoporphyrin was copied into the model and, finally, an iron atom was inserted.

MD simulations

Models of the WT and variant MFCh with haem were optimized and equilibrated by the GROMACS package [24], using the GROMOS96 force field (version 43A1) [25], in the periodic boundary conditions regime. For the haem molecule, the HEME topology was applied. The same force field has been successfully used before, to study haem-containing enzymes, for example cytochrome *c* [26]. Initially, the structures were solvated in a box of simple point charge (SPC) [27] water molecules of 90 Å × 90 Å × 90 Å. The total charge of the WT model is +6; protonation of titrable residues (shown in Table S1) was chosen on the basis of the ability to form hydrogen bonds with neighbouring residues, exposure to the solvent, etc. Selected water molecules in the WT and H209N model were replaced with 38 sodium and 42 chlorine atoms, resulting in a salt concentration around 0.1 M and the system being neutral. In the E289Q model, 38 sodium and 43 chlorine atoms were inserted. Next, the model was optimized with the steepest-descent method until the maximum force reached 2,000 kJ mol^{-1} nm^{-1}. Heavy atoms of the protein were constrained in their initial position by a harmonic potential. Next, the system was equilibrated for 100 ps with positional constraints on heavy atoms of the protein. All bond lengths were constrained using the LINCS algorithm [28]. The time step used was 2 fs. Electrostatic interactions were evaluated using the fast particle-mesh Ewald (PME) method [29] with a 9-Å cut-off between the direct and reciprocal sum and cubic interpolation of the charges. Van der Waals (Lennard-Jones) interactions were calculated using a twin-range cut-off set to 9 and 14 Å. The neighbour list was regenerated every ten steps. Equilibration and further simulation of the system was conducted within the NpT ensemble. During the equilibration phase, the Berendsen thermostat was used [30], with a reference temperature of

300 K and a coupling constant of 0.1 ps. The pressure was maintained using the Berendsen barostat [30], with a reference pressure of 1 bar, a coupling constant of 1 ps and compressibility of 4.5×10^{-5} bar^{-1}. After the equilibration, the system was simulated for 21 ns using a time step of 2 fs. This production run was set up in a manner similar to that for the equilibration phase, with some differences, i.e. no constraints were applied to the system; translation and rotation of the protein were verified every five steps and the system was adjusted to cancel possible drift or spin of the molecule; constant temperature was maintained using the Nosé–Hoover thermostat [31, 32], with a coupling constant of 0.5 ps and a reference temperature of 300 K; and constant pressure was preserved using the Parrinello–Rahman barostat [33], with a coupling constant of 4 ps, a reference pressure of 1 bar and compressibility set to 4.5×10^{-5} bar^{-1}.

In all the simulations mentioned above, a monomeric form of the protein was considered, although the in vivo form is probably homodimeric [34]. In fact, X-ray structures for human ferrochelatase reveal an homodimer [9], and as MFCh shares a high amino acid sequence similarity with its human counterpart, it seems reasonable to assume that the mouse enzyme also has a homodimeric quaternary structure. From the X-ray structure of the human enzyme it is also known that the active site is located relatively far from the interface.

In the attempt to test possible sources of ambiguity, alternative positions of the haem molecule were considered. The models of WT, H209N and E289Q assume position analogous to the human structure (which seems reasonable, owing to a very high sequence identity). Two Additional orientations of haem in the WT active site were also tested, differing from the 2HRC model by the haem molecule being twisted and flipped within its plane (other orientations were disregarded, due to a steric clash). Each of these alternative conformers (WTa and WTb) were simulated starting from the final geometry of the WT (thus saving the long equilibration time). The set-up was identical to that for the simulation of the WT. In WTa, propionate groups of the haem are pointing towards the entrance of the active site, in WTb they are pointing towards the back of the active site, whereas in the WT they are positioned sideways.

Data analysis

From each trajectory, one snapshot was selected, and the snapshots of the variant forms were aligned with the WT structure by minimizing the RMS distance of main-chain and haem atoms. After that, the RMS distance between atoms of the WT and the variant forms was compared. The snapshots were chosen in the following way: the structure was averaged over the production period; then the RMS deviation of the protein and the haem molecule was calculated along the trajectory, with respect to the average position; finally, a snapshot having lowest RMS value (i.e. being closest to the average structure) was selected, at 13,529 ps for the WT, at 14,053.4 ps for H209N and at 12,191 ps for E289Q. Additionally, for validation purposes, a second set with slightly higher RMS value was selected: at 18,123.2 ps for the WT, at 9,310.4 ps for H209N and at 8,402.4 ps for E289Q. For each trajectory, in the given period, RMS fluctuations of C_α atoms with respect to the average position were calculated, to find regions where the mutation contributed to an increase or decrease in the fluctuations. The structure of the active site and the influence of the mutations on the geometry and distortion of the haem macrocycle were analysed in detail: the distortion of the haem was analysed by calculating the average distance of each atom from the plane surface and per-atom RMS deviation from planarity. The plane equation was calculated for the 25 numbered atoms shown in Fig. 1, using a least-squares-fit method [35]. The distortion of the macrocycle was also estimated using the normal-coordinate structural decomposition (NSD) method, developed by Jentzen et al. [36] Prior to NSD calculations, representative structures of the haem molecule were searched for each of the complexes (WT, H209N, E289Q). This was accomplished by calculating the averaged structure of haem over the production period and selecting a snapshot having the lowest RMS deviation value, compared with this averaged structure. These representative structures were subjected to NSD analysis. Finally, selected contacts between residues in the active site and propionate groups of haem were analysed by calculating the radial distribution function (RDF) for heavy atoms forming each hydrogen bond. Similar analysis was performed for the pair of residues 209 and 289, which are subject to mutation, and two residues (Met22 and His209) that can interact with the iron atom.

Results and discussion

The mutations do not seem to alter the general structure of the protein significantly. The most pronounced changes take place in the loop regions, near residues 304 and 348 in both variants (Figs. 3, 4). Residue 348 is near the place occupied by the [2Fe–2S] cluster. Additionally, there is significant difference in the structure near residue 253, particularly in the E289Q variant. This is a proline residue in another loop region, located at the entrance to the active pocket. In the E289Q variant, this loop is covering the active site much more than in the WT and interacts with Arg61, which could possibly prevent the release of haem

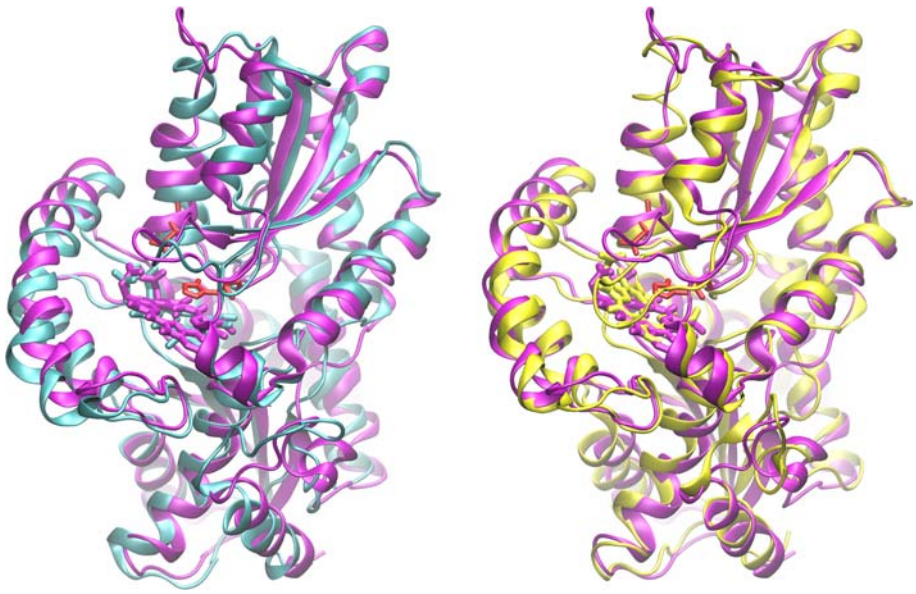

Fig. 3 Superposition of the H209N (*cyan*) and E289Q (*yellow*) variants with the wild-type (WT) form (*magenta*) of the ferrochelatase, based on a least-squares fit of the main-chain and haem atoms. The position of the replaced amino acids is shown in *red*

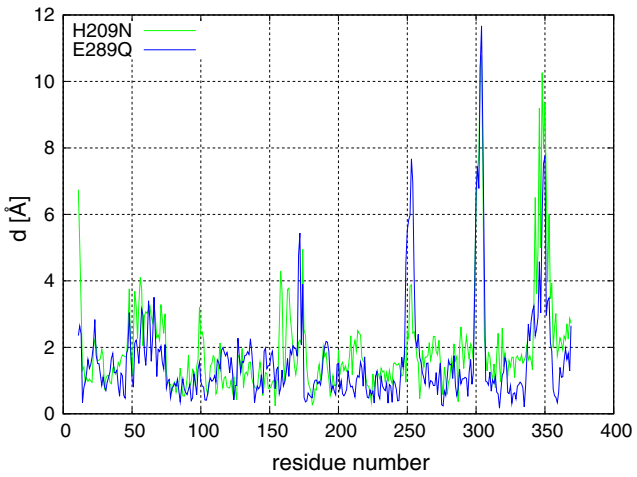

Fig. 4 Distance between C_α atoms in variant and WT models calculated after least-squares fit of the snapshots from the molecular dynamics simulations

from the active site. These differences in the structure of WT and variant MFCh are not specific for the snapshots chosen; Fig. S4 shows that they can also be observed for other selections of snapshots.

The mutations also have a certain, however not large, impact on the overall stability of the structure. In Fig. S5, the RMS fluctuations of the C_α atoms are depicted. The regions in which the structure becomes stiffer or more flexible due to the mutations are shown in Fig. 5. These are only the loop regions, but it is worth mentioning that loop 250–258, which partially covers the entrance to the active site, becomes more rigid in the E289Q variant. Also, the 302–307 fragment, which is quite flexible in the WT and the H209N variant, becomes rigid in E289Q. This fragment is located in the helix that incorporates the catalytic residue Glu289; therefore, its flexibility may be related to the mutation and activity of the variant enzyme.

Figure 6 shows the interaction energy of the haem molecule with the WT and variant enzymes. According to the graph, the E289Q variant interacts with the haem more strongly than the WT or H209N, which in turn exhibit a similar amount of interaction energy. Increased interaction in the E289Q variant may handicap the release of the product and slow down the reaction, as previously observed [16, 17]. Owing to the fact that the particle-mesh Ewald method was used, the interactions are split into short-range and long-range components and the long-range Coulomb component is not included in this sum. The cut-off distance for the electrostatic interactions is 9 Å; therefore, the omitted long-range Coulomb interaction should not affect the relative value of the sum.

In the progress of the simulation, the orientation of the haem molecule in WT MFCh diverged only a little, remaining similar to the orientation in the X-ray geometry of the human enzyme [9], which was used as an initial model. Note, that the orientation of PPIX in *B. subtilis* ferrochelatase [37] (PDB code 1C1H) is significantly different. In the latter structure, the propionates point out of the active site, whereas in MFCh the haem molecule is rotated and propionates can form hydrogen bonds with several active-site residues, including Arg61, Tyr69, Ser76 and Ser249 (Figs. 7, 8). It is possible that these residues are responsible not only for the proper orientation of PPIX, but also for the macrocycle distortion. Met22 is positioned under the haem molecule, whereas the catalytic His209 coordinates the ferrous ion from above. The position of the haem molecule in the active site is similar in both variants; however, in the E289Q variant, the propionates of the haem molecule are tilted in the opposite directions (up and down

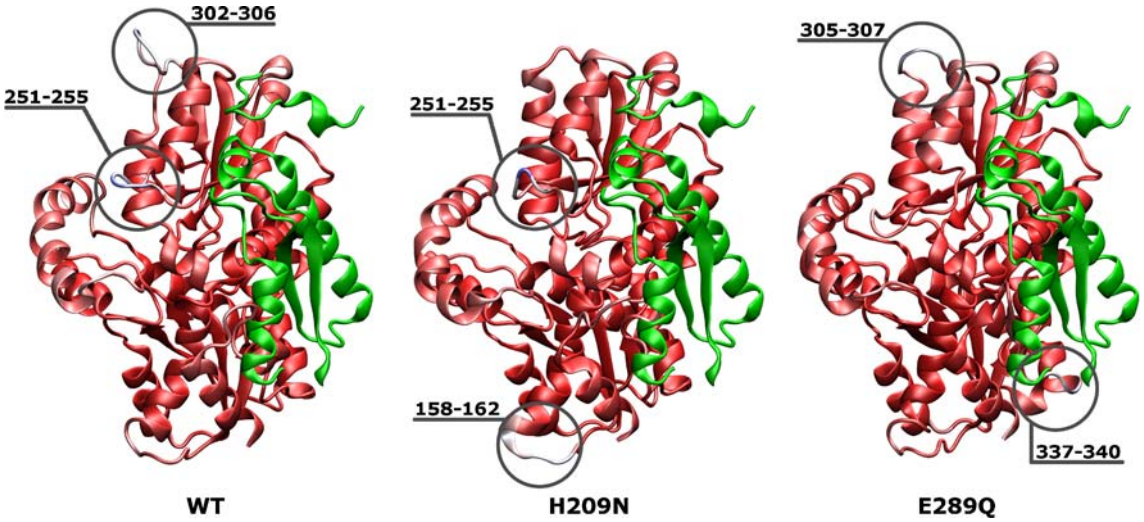

Fig. 5 Colour-coded regions of increased flexibility (most flexible regions in *blue*, also marked with *circles*) in WT and variant MFCh. Note that loop 251–255 becomes stabilized in E289Q. See also Fig. S5. *Green* indicates the hypothetical position of the monomer–monomer interface (fragment of the second monomer), based on the human enzyme

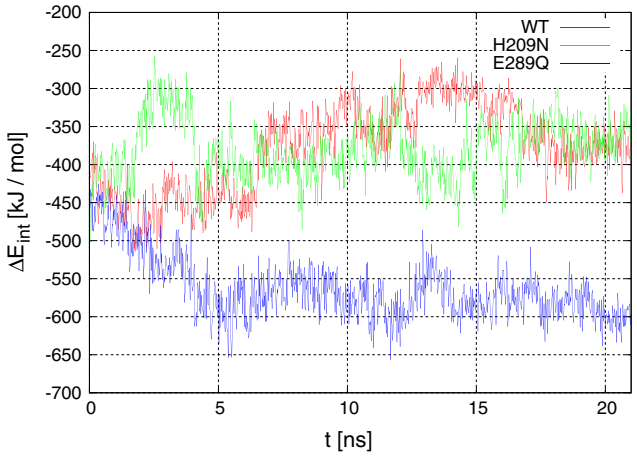

Fig. 6 Interaction energy between protein and haem molecule including short-range Coulomb and Lennard-Jones (short-range and long-range) interactions

the plane), whereas in the WT and H209N, both propionates are tilted upwards, to the side occupied by His209 and Glu289. The propionate groups are coordinated by Arg61 and Ser76 in the WT, by Arg61, Tyr69 and Ser76 in the H209N variant and by Arg61, Tyr69, Ser76, Ser249 and Gln289 in the E289Q variant. As can be seen from the RDFs in Fig. 8, the propionates in E289Q are strongly coordinated by five residues, which could be the reason for the stronger interaction between the protein and the haem. The function of the propionates of the haem molecule has been investigated in other, similar systems, including cytochrome *c* [26, 38]. Furlan et al. [39] used Car–Parrinello MD to study a truncated model of the active site. The influence of the propionates on the rotational freedom of His18 (analogous to His209 in ferrochelatase) was observed. Even more interesting, the authors found a necessity to include another ligand (fragment of Pro30), which forms a hydrogen bond with the same histidine, to ensure separation of the charges of propionates and histidine. Indeed, in WT, WTa and E289Q models of MFCh the contact between propionates and His209 is not observed and His209 forms hydrogen bonds with other residues.

The orientation of the haem molecule in the MFCh models presented here (WT, H209N and E289Q) is similar to the orientation of PPIX and haem in X-ray structures of human ferrochelatase [9]. Haem can also bind in the active site in an orientation which is flipped and rotated by approximately 45° (compare WT and WTb in Fig. S9), suggesting that there is some conformational freedom—at least in the product complex. On the other hand, *N*-methylmesoporphyrin and 2,4-disulphonic acid dihydrochloride bound in the active site of the crystal structure of the ferrochelatase from *B. subtilis* appear to be rotated by approximately 100° and are not buried in the active site as deeply as in mammal ferrochelatases [12, 37]. According to the recent work of Karlberg et al. [12], this different orientation in *B. subtilis* may be sufficient to provide the necessary distortion of the porphyrin and catalyse the reaction. The same work explains the difference in the binding mode between the mammal and bacterial enzymes in terms of steric hindrance caused by one of the helices. This is accompanied by an altered coordination of the propionates, resulting from differences in the secondary structure.

The catalytic role of the ferrochelatase is to distort PPIX, which makes it easier to detach the protons from the nitrogen atoms and exposes the electron pairs of the nitrogens, enabling insertion of the ion [7, 15]. For that

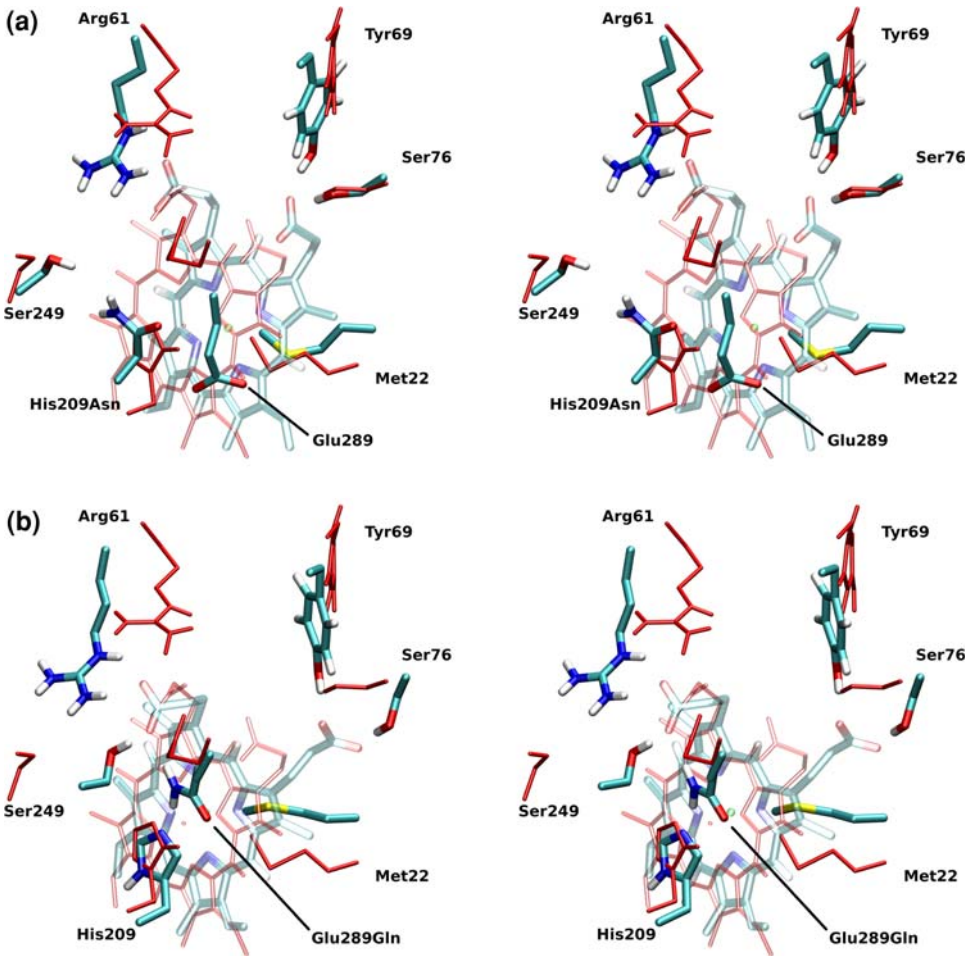

Fig. 7 Stereo view of the active site of variants H209N (**a**) and E289Q (**b**) compared with the structure of the active site of the WT (*thin lines*); based on snapshots from the molecular dynamics simulations

reason, it is particularly interesting to compare the planarity of the haem molecule in variant MFCh with the model of WT enzyme. Figure 9 shows the average distance of the haem atoms from the molecule plane (in other words, the non-planarity of the haem bound in the active site) and Fig. S6 shows RMS distances of haem atoms from the plane, which illustrate how much the molecule can be distorted. Both graphs show that the haem molecule bound in the active site of WT protein is much more planar and much stiffer (lower RMS values) than in the variant proteins. The maximum average deviation from planarity is less than 0.3 Å and the maximum RMS distance from the plane is around 0.3 Å. This result agrees very well with the theory that ferrochelatase preferentially stabilizes "domed" geometry of the protoporphyrin in the transition state, but the product—after the insertion of the ferrous ion—is planar and as such would be destabilized and easily released from the active site. On the other hand, the variant enzymes enforce distortion in the haem molecule, which would shift the chemical equilibrium towards the reactant state. The largest average value of the distortion from planarity of a single atom in the H209N and E289Q variants is around 0.5 Å on atoms 9 and 21 of the haem molecule and around 0.4 Å on atoms 3 and 15. The haem molecule in both variants exhibits mostly a "saddling" distortion. This can be seen in the "per-atom" analysis (Fig. 9), as well as in the NSD results (Fig. 10). In this form of distortion, the atoms that are most tilted are the outer carbons of the pyrrole rings. The opposite pyrrole rings are tilted in the same direction, i.e. rings A and C are tilted up and B and D are tilted down. In the H209N variant, the ferrous ion is pulled out of the macrocycle more than in the E289Q variant and the WT (compare atom 25 in Figs. 9, S6). Apparently, His209, placed in the WT and E289Q over the iron atom, coordinates it with the nitrogen atom of the imidazole, preventing expulsion of the ion and distortion of the macrocycle in the product complex.

Mutation of the two active-site residues, His209 and Glu289, alters the network of hydrogen bonds between haem and WT protein (Fig. 8). Five residues in the active site are able to form hydrogen bonds with propionate groups of haem. Arg61 interacts in the WT, as well as in variant proteins. The RDF of Arg61 (Fig. 8) has two peaks, since typically a hydrogen bond is formed with one of the

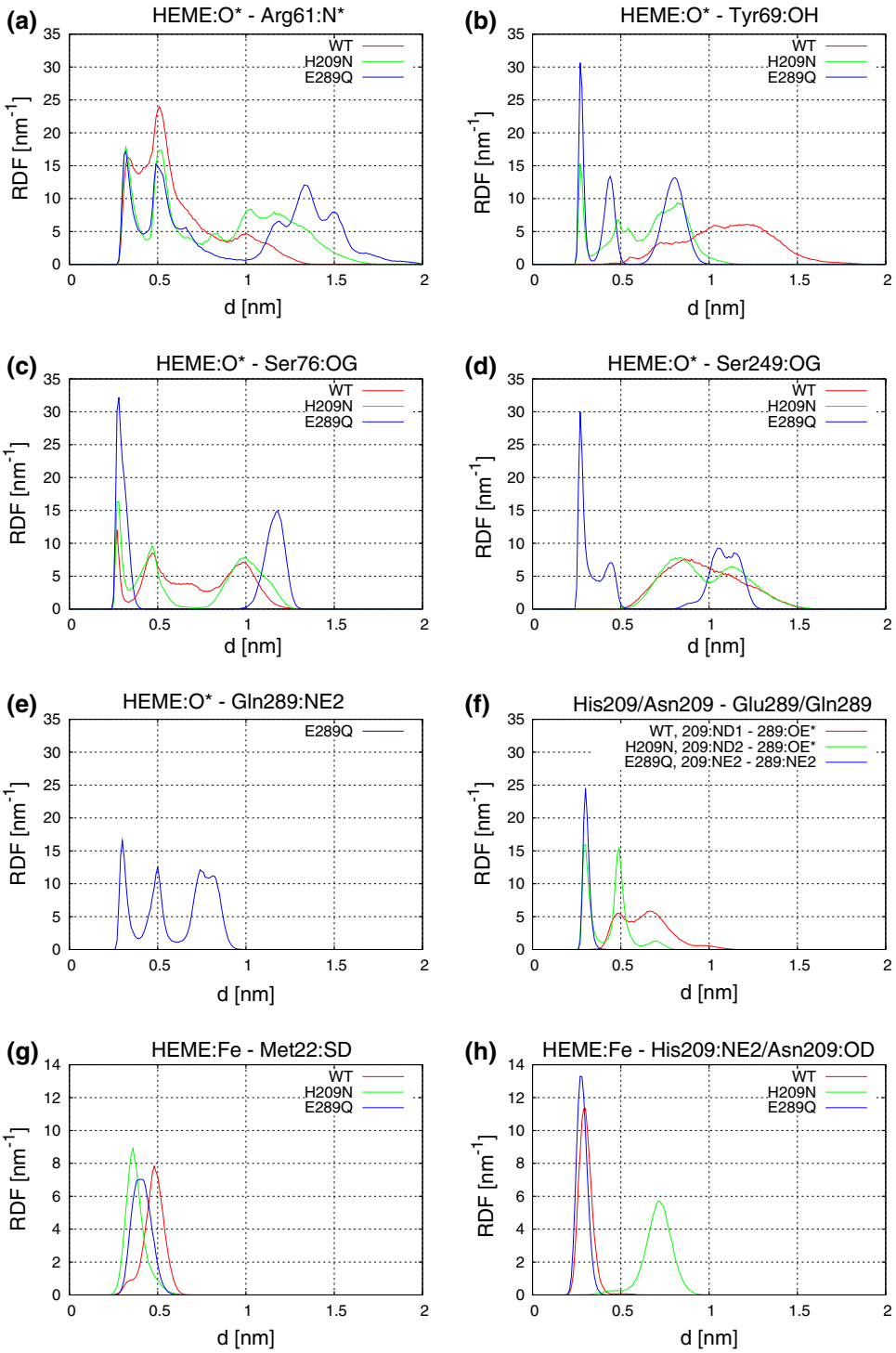

Fig. 8 Radial distribution functions (*RDF*) of selected contacts between active-site residues and propionate groups of the haem molecule (**a**–**e**), residues 209 and 289 (**f**) and active-site residues and the iron atom (**g**–**h**)

N_ω atoms, whereas the other one remains within 5-Å distance. In H209N and E289Q variants, a new contact with Tyr69 emerges and competes with Ser76 for the interaction with one propionate group. Ser76 makes a contact with propionate groups, which is not affected by the mutations, whereas Ser249 forms a hydrogen bond with propionate group only in E289Q. Only two contacts remain intact in both mutants, namely the hydrogen bonds formed by Arg61 and Ser76 with one of the propionate groups of haem. Mutation of Glu289 introduces another interaction—the mutated Gln289 periodically forms a third hydrogen bond with the propionate coordinated by Arg61 and Ser249. Finally, the two residues 209 and 289 interact with one another through hydrogen bonds, but only in the variant proteins. In general, the RDFs show that the hydrogen-bond network is much stronger in the E289Q variant. For

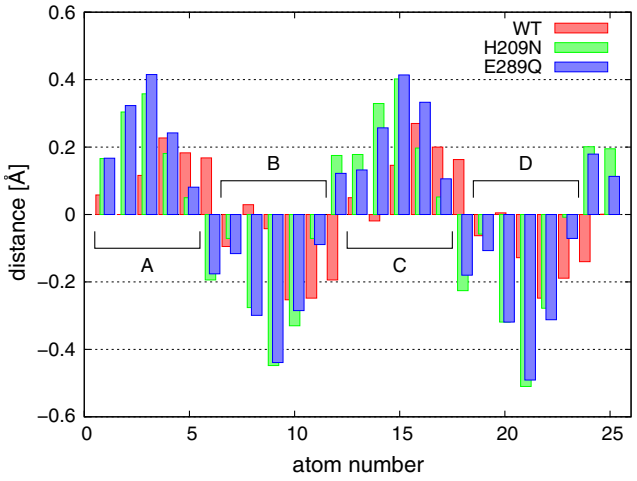

Fig. 9 Average distance of haem atoms from the macrocycle plane. Atom numbers are shown in Fig. 1

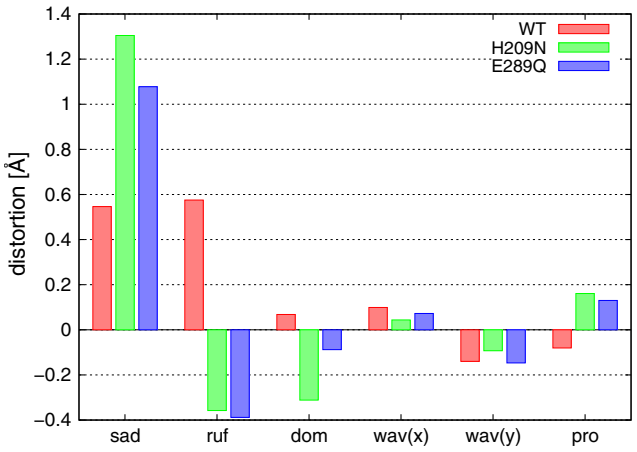

Fig. 10 Normal-coordinate structural decomposition of WT and variant forms of the ferrochelatase isolated from mouse into six types of deformations: saddling (*sad*), ruffling (*ruf*), doming (*dom*), waving [*wav (x)*, *wav (y)*] and propelling (*pro*) [36]

the six contacts shown in this figure, only E289Q possess hydrogen bonds in all of them. The WT does not form a hydrogen bond with Tyr69 and Ser249, H209N does not have the contact with Ser249 and only E289Q can make an additional hydrogen bond with the mutated residue. Therefore, the increased interaction observed in Fig. 6 cannot be explained only by the depletion of the charge in this mutant—apparently, structural changes caused by the mutation enable additional contacts, which are not possible in the WT and H209N. This additional coordination of the propionate groups results in stronger binding of the product and presumably also of the reactant complex, which would explain experimental observations of endogenous and specifically bound PPIX in the E289Q MFCh variant [16, 17]. It could explain also significant differences in the resonance Raman spectra of PPIX bound to the WT and to the E289Q variant [13]. It also affects the orientation of the macrocycle, which in the E289Q variant is displaced towards the "entrance" of the active site, compared with the WT and H209N (Fig. 7).

Simulations of the WT enzyme conformers (WT, WTa, WTb) show that there is space for a certain freedom of orientation of the haem in the active site. In WTb, one the propionates forms additional hydrogen bonds with His209, Gln248 and His287, whereas the hydrogen bond with Ser76 (found in the WT) is not present (Fig. S7). In WTb, there is also a sodium cation, coordinated by one of the propionates and Glu289 (not present in the WT and WTa). The energy of the interaction between haem and protein is slightly higher in WTb (-385 kJ mol^{-1}) than in the WT (-350 kJ mol^{-1}). On the other hand, in WTa, the interaction between haem and enzyme is weaker (-339 kJ mol^{-1}) and the porphyrin is displaced from the active site (note the position of Met22 and His209 in Fig. S9) and the saddling cannot be observed (Fig. S8). It seems that WTa corresponds more to a situation where haem is leaving the active pocket of the enzyme (although on the time scale of the simulation this cannot be observed). This is also supported by the general picture of the hydrogen-bond network in these three models (Fig. S7)—in the case of WTb the peaks are mostly narrow, whereas in the case of WTa they are broad and low (indicating large fluctuations). In WTa, only Ser249 forms a hydrogen bond with propionates of the haem and the distance from catalytic His209 is significantly enlarged.

Conclusions

MD simulations of the monomeric WT and variant MFCh prove that mutations of the active-site residues, His209 and Glu289, have an influence on the haem and, presumably, PPIX distortion. The impact on the macrocycle distortion appears to be quite complex; the mutations cause subtle changes in the geometry of the neighbourhood, which in turn alters the coordination of the propionate groups of protoporphyrin by several residues, including Tyr69, Ser76 and Ser249. On the other hand, a direct relation between the strength of the interaction (measured in the interaction energy) and the distortion of the macrocycle could not be found. In the E289Q variant, the haem molecule forms more contacts and interacts more strongly with the protein than in the WT and H209N, but it is the H209N mutation that causes the largest distortion. It seems that His209, apart from being implicated in ferrous ion binding [12, 40] and proton extraction [8], also has a role in the induction of the planar geometry of the product. Different residues are responsible for coordination and orientation of the porphyrin in the mouse and bacterial enzymes.

Acknowledgments Calculations were carried out at the Wrocław Centre for Networking and Supercomputing. B.S. would like to thank the Fundação para a Ciência e a Tecnologia (Lisbon) for fellowship no. SFRH/BPD/38809/2007. Also, B.S. would like to thank Edyta Dyguda-Kazimierowicz for expertise on homology modelling and Miguel Jorge for useful discussions about MD simulations.

References

1. Loew GH, Harris DL (2000) Chem Rev 100:407–420
2. Sun J, Brand M, Zenke Y, Tashiro S, Groudine M, Igarashi K (2004) Proc Natl Acad Sci USA 101:1461–1466
3. Atamna H, Frey II WH (2004) Proc Natl Acad Sci USA 101:11153–11158
4. Ajioka RS, Phillips JD, Kushner JP (2006) Biochim Biophys Acta Mol Cell Res 1763:723–736
5. Ferreira GC, Moura JJG, Franco R (1999) Iron metabolism: inorganic biochemistry and regulatory mechanisms. Wiley, New York
6. Dailey HA, Dailey TA, Wu CK, Medlock AE, Wang KF, Rose JP, Wang BC (2000) Cell Mol Life Sci 57:1909–1926
7. Al-Karadaghi S, Franco R, Hansson M, Shelnutt JA, Isaya G, Ferreira GC (2006) Trends Biochem Sci 31:135–142
8. Dailey HA, Wu CK, Horanyi P, Medlock AE, Najahi-Missaoui W, Burden AE, Dailey TA, Rose J (2007) Biochemistry 46:7973–7979
9. Medlock A, Swartz L, Dailey TA, Dailey HA, Lanzilotta WN (2007) Proc Natl Acad Sci USA 104:1789–1793
10. Al-Karadaghi S, Hansson M, Nikonov S, Jönsson B, Hederstedt L (1997) Structure 5:1501–1510
11. Wu CK, Dailey HA, Rose JP, Burden A, Sellers VM, Wang BC (2001) Nat Struct Biol 8:156–160
12. Karlberg T, Hansson MD, Yengo RK, Johansson R, Thorvaldsen HO, Ferreira GC, Hansson M, Al-Karadaghi S (2008) J Mol Biol 378:1074–1083
13. Franco R, Ma JG, Ferreira GC, Shelnutt JA (2000) Biochemistry 39:2517–2529
14. Shi Z, Ferreira GC (2004) J Biol Chem 279:19977–19986
15. Sigfridsson E, Ryde U (2003) J Biol Inorg Chem 8:273–282
16. Franco R, Pereira AS, Tavares P, Mangravita A, Barber MJ, Moura I, Ferreira GC (2001) Biochem J 356:217–222
17. Franco R, Bai G, Prosinecki V, Abrunhosa F, Ferreira GC, Bastos M (2005) Biochem J 386:599–605
18. Hansson MD, Karlberg T, Rahardja MA, Al-Karadaghi S, Hansson M (2007) Biochemistry 46:87–94
19. Dailey HA (1987) Ann N Y Acad Sci 514:81–86
20. Šali A, Blundell TL (1993) J Mol Biol 234:779–815
21. Carninci P, Kasukawa T, Katayama S, Gough J, Frith MC, Maeda N, Oyama R, Ravasi T, Lenhard B, Wells C, Kodzius R, Shimokawa K, Bajic VB, Brenner SE, Batalov S, Forrest ARR, Zavolan M, Davis MJ, Wilming LG, Aidinis V, Allen JE, Ambesi-Impiombato A, Apweiler R, Aturaliya RN, Bailey TL, Bansal M, Baxter L, Beisel KW, Bersano T, Bono H, Chalk AM, Chiu KP, Choudhary V, Christoffels A, Clutterbuck DR, Crowe ML, Dalla E, Dalrymple BP, de Bono B, Gatta GD, di Bernardo D, Down T, Engstrom P, Fagiolini M, Faulkner G, Fletcher CF, Fukushima T, Furuno M, Futaki S, Gariboldi M, Georgii-Hemming P, Gingeras TR, Gojobori T, Green RE, Gustincich S, Harbers M, Hayashi Y, Hensch TK, Hirokawa N, Hill D, Huminiecki L, Iacono M, Ikeo K, Iwama A, Ishikawa T, Jakt M, Kanapin A, Katoh M, Kawasawa Y, Kelso J, Kitamura H, Kitano H, Kollias G, Krishnan SPT, Kruger A, Kummerfeld SK, Kurochkin IV, Lareau LF, Lazarevic D, Lipovich L, Liu J, Liuni S, McWilliam S, Babu MM, Madera M, Marchionni L, Matsuda H, Matsuzawa S, Miki H, Mignone F, Miyake S, Morris K, Mottagui-Tabar S, Mulder N, Nakano N, Nakauchi H, Ng P, Nilsson R, Nishiguchi S, Nishikawa S, Nori F, Ohara O, Okazaki Y, Orlando V, Pang KC, Pavan WJ, Pavesi G, Pesole G, Petrovsky N, Piazza S, Reed J, Reid JF, Ring BZ, Ringwald M, Rost B, Ruan Y, Salzberg SL, Sandelin A, Schneider C, Schnbach C, Sekiguchi K, Semple CAM, Seno S, Sessa L, Sheng Y, Shibata Y, Shimada H, Shimada K, Silva D, Sinclair B, Sperling S, Stupka E, Sugiura K, Sultana R, Takenaka Y, Taki K, Tammoja K, Tan SL, Tang S, Taylor MS, Tegner J, Teichmann SA, Ueda HR, van Nimwegen E, Verardo R, Wei CL, Yagi K, Yamanishi H, Zabarovsky E, Zhu S, Zimmer A, Hide W, Bult C, Grimmond SM, Teasdale RD, Liu ET, Brusic V, Quackenbush J, Wahlestedt C, Mattick JS, Hume DA, Kai C, Sasaki D, Tomaru Y, Fukuda S, Kanamori-Katayama M, Suzuki M, Aoki J, Arakawa T, Iida J, Imamura K, Itoh M, Kato T, Kawaji H, Kawagashira N, Kawashima T, Kojima M, Kondo S, Konno H, Nakano K, Ninomiya N, Nishio T, Okada M, Plessy C, Shibata K, Shiraki T, Suzuki S, Tagami M, Waki K, Watahiki A, Okamura-Oho Y, Suzuki H, Kawai J, Hayashizaki Y (2005) Science 309:1559–1563
22. Laskowski RA, MacArthur MW, Moss DS, Thornton JM (1993) J Appl Crystallogr 26:283–291
23. Medlock AE, Dailey TA, Ross TA, Dailey HA, Lanzilotta WN (2007) J Mol Biol 373:1006–1016
24. van der Spoel D, Lindahl E, Hess B, Groenhof G, Mark AE, Berendsen HJC (2005) J Comp Chem 26:1701–1718
25. van Gunsteren WF, Billeter SR, Eising AA, Hünenberger PH, Krüger P, Mark AE, Scott WRP, Tironi IG (1996) Biomolecular simulation: the GROMOS96 manual and user guide. Hochschulverlag AG an der ETH Zürich, Zürich, Switzerland
26. Smith LJ, Davies RJ, van Gunsteren WF (2006) Proteins Struct Funct Bioinformatics 65:702–711
27. Berendsen HJC, Postma JPM, van Gunsteren WF, Hermans J (1981) In: Pullman B (ed) Intermolecular forces. Reidel, Dordrecht, pp 331–342
28. Hess B, Bekker H, Berendsen HJC, Fraaije JGEM (1997) J Comput Chem 18:1463–1472
29. Essman U, Perela L, Berkowitz ML, Darden T, Lee H, Pedersen LG (1995) J Chem Phys 103:8577–8592
30. Berendsen HJC, Postma JPM, DiNola A, Haak JR (1984) J Chem Phys 81:3684–3690
31. Nosé S (1984) Mol Phys 52:255–268
32. Hoover WG (1985) Phys Rev A 31:1695–1697
33. Parrinello M, Rahman A (1981) J Appl Phys 52:7182–7190
34. Straka JG, Bloomer JR, Kempner ES (1991) J Biol Chem 266:24637–24641
35. Schomaker V, Waser J, Marsh RE, Bergman G (1959) Acta Crystallogr 12:600–604
36. Jentzen W, Song XZ, Shelnutt JA (1997) J Phys Chem B 101:1684–1699
37. Lecerof D, Fodje M, Hansson A, Hansson M, Al-Karadaghi S (2000). J Mol Biol 297:221–232
38. La Penna G, Furlan S, Banci L (2007) J Biol Inorg Chem 12:180–193
39. Furlan S, La Penna G, Banci L, Mealli C (2007) J Phys Chem B 111:1157–1164
40. Ferreira GC, Franco R, Mangravita A, George GN (2002). Biochemistry 41:4809–4818
41. Larkin MA, Blackshields G, Brown NP, Chenna R, McGettigan PA, McWilliam H, Valentin F, Wallace IM, Wilm A, Lopez R, Thompson JD, Gibson TJ, Higgins DG (2007) Bioinformatics 23:2947–2948
42. Waterhouse AM, Procter JB, Martin DMA, Clamp M, Barton GJ (2009) Bioinformatics 25:1189–1191